1 **Proteome constraints reveal targets for improving microbial fitness in nutrient-rich**
2 **environments**
3

4 Author list:
5 Yu Chen[1,2,10], Eunice van Pelt-KleinJan[3,4,10], Berdien van Olst[3,5,6], Sieze Douwenga[3,4], Sjef
6 Boeren[3,6], Herwig Bachmann[3,4,7], Douwe Molenaar[3,4], Jens Nielsen[1,2,8,9,11], and Bas Teusink[3,4,11]
7

8 Affiliation:
9 [1]Department of Biology and Biological Engineering, Chalmers University of Technology, SE-412
10 96 Gothenburg, Sweden
11 [2]Novo Nordisk Foundation Center for Biosustainability, Chalmers University of Technology, SE-
12 41296 Gothenburg, Sweden
13 [3]TiFN, P.O. Box 557, NL6700AN Wageningen, the Netherlands
14 [4]Systems Biology Lab, Amsterdam Institute of Molecular and Life Sciences (AIMMS), Vrije
15 Universiteit Amsterdam, NL1081HZ Amsterdam, The Netherlands
16 [5]Host-Microbe Interactomics, Wageningen University & Research, NL6708WD Wageningen,
17 The Netherlands
18 [6]Laboratory of Biochemistry, Wageningen University & Research, NL6708WE Wageningen,
19 The Netherlands
20 [7]NIZO Food Research, NL6718ZB Ede, The Netherlands
21 [8]Novo Nordisk Foundation Center for Biosustainability, Technical University of Denmark,
22 DK2800 Kgs. Lyngby, Denmark
23 [9]BioInnovation Institute, DK2200 Copenhagen N, Denmark
24 [10]These authors contributed equally: Yu Chen, Eunice van Pelt-KleinJan
25 [11]These authors jointly supervised this work: Jens Nielsen, Bas Teusink
26

27 ORCID ID:
28 Yu Chen (https://orcid.org/0000-0003-3326-9068)
29 Eunice van Pelt-KleinJan (https://orcid.org/0000-0002-6590-652X)
30 Berdien van Olst (https://orcid.org/0000-0001-8596-0171)
31 Sieze Douwenga (https://orcid.org/0000-0003-3604-7524)
32 Sjef Boeren (https://orcid.org/0000-0002-0847-8821)
33 Herwig Bachmann (https://orcid.org/0000-0002-8224-0993)
34 Douwe Molenaar (https://orcid.org/0000-0001-7108-4545)
35 Jens Nielsen (https://orcid.org/0000-0002-9955-6003)
36 Bas Teusink (https://orcid.org/0000-0003-3929-0423)
37
38

1 **Cells adapt to different conditions via gene expression that tunes metabolism and stress**
2 **resistance for maximal fitness. Constraints on cellular proteome may limit such expression**
3 **strategies and introduce trade-offs[1]; Resource allocation under proteome constraints has**
4 **emerged as a powerful paradigm to explain regulatory strategies in bacteria[2]. It is unclear,**
5 **however, to what extent these constraints can predict evolutionary changes, especially for**
6 **microorganisms that evolved under nutrient-rich conditions, i.e., multiple available nitrogen**
7 **sources, such as the lactic acid bacterium *Lactococcus lactis*. Here we present an approach**
8 **to identify preferred nutrients from integration of experimental data with a proteome-**
9 **constrained genome-scale metabolic model of *L. lactis* (pcLactis), which explicitly accounts**
10 **for gene expression processes and associated constraints. Using glucose-limited chemostat**
11 **data[3], we identified the uptake of glucose and arginine as dominant constraints, whose**
12 **pathway proteins were indeed upregulated in evolved mutants. However, above a growth**
13 **rate of 0.5 h^{-1}, pcLactis suggests that available enzymes function at their maximum capacity,**
14 **which allows an increase in growth rate only by altering gene expression to change**
15 **metabolic fluxes, as was mainly observed for arginine metabolism. Thus, our integrative**
16 **analysis of flux and proteomics data with a proteome-constrained model is able to identify**
17 **and explain the constraints that form targets of regulation and fitness improvement in**
18 **nutrient-rich growth environments.**

19
20 The fitness of unicellular organisms is determined by adaptions to environmental conditions[1],
21 and is optimized by regulating metabolic processes that generally lead to higher growth rates[4].
22 Growth rates are finite, as the metabolic processes supporting growth are constrained
23 through limits imposed by external conditions, e.g., nutrient availability, and internal factors
24 that relate to cell morphology, enzyme kinetics and physicochemical properties such as
25 solvent capacities. In particular, constraints on the allocation of the proteome, due to limited
26 membrane area or intracellular volume, have aided to understand metabolic adaptions of
27 microorganisms[5–7], specifically, the overflow metabolism in *Escherichia coli*[8–10] and the
28 Crabtree effect in *Saccharomyces cerevisiae*[11–13].

29
30 However, much less is known about metabolic adaptations in other organisms, and especially
31 those cultivated under conditions with multiple available substrates, such as in nutrient-rich
32 environments like the gut or food. It was previously shown that anaerobic overflow
33 metabolism in the lactic acid bacterium *L. lactis* is not accompanied by changes in associated
34 protein levels[3], questioning the generality of the resource allocation paradigm. However,
35 changes in gene expression were observed, in particular in amino acid metabolism, prompting
36 us to revisit the cellular economics of *L. lactis*.

37
38 *L. lactis* is an important model lactic acid bacterium and work horse for the dairy industry -
39 production of cheese in particular[14,15]. Many strains are auxotrophic for at least five amino
40 acids[16,17], and thus *L. lactis* strains are grown in nutrient-rich environments where amino acids
41 are usually in excess. Many of these amino acids participate not only in anabolic processes but
42 also their catabolism can contribute to energy metabolism[18]. For example, arginine catabolism
43 directly yields ATP and is tightly regulated[19], while other amino acids can contribute to pH or
44 redox homeostasis, saving ATP-costly alternatives[20]. It is, however, not known whether
45 proteome constraints guide choices in non-sugar substrates, e.g., amino acids.

46

1   We therefore developed pcLactis, a proteome-constrained genome-scale metabolic model of
2   *L. lactis*. We first updated a published genome-scale metabolic model for *L. lactis* MG1363[21,22]
3   mostly by adding transport capacities and gene protein reaction associations (Supplementary
4   Data 1). Second, we added the gene expression processes, including transcription, stable RNA
5   cleavage, mRNA degradation, tRNA modification, rRNA modification, tRNA charging,
6   ribosomal assembly, translation, protein maturation and assembly, and protein degradation
7   (Fig 1a). By integrating the two reconstructions, we obtained pcLactis, which accounts for 725
8   protein-coding genes and 81 RNA genes in *L. lactis* MG1363. According to the PaxDb
9   database[23], pcLactis accounts for approximately 60% of the total proteome by mass
10 (Supplementary Data 2). The model's proteome therefore includes 40% unmodelled protein
11 of average amino acid composition. We constrain metabolic fluxes by enzyme levels, following
12 standard enzyme kinetics; Enzyme levels follow from mass balancing synthesis rate and
13 degradation and dilution by growth (Fig 1b). Total protein synthesis rates are constrained by
14 ribosomal translation capacity and by a total proteome constraint, i.e., a maximum size of the
15 proteome. We use inactive enzyme, again with average amino acid composition, to fill up the
16 total proteome in cases of low enzymatic activity, e.g. at low growth rates. Inactive enzyme
17 can be seen as the excess capacity of the total modelled proteome.
18
19 We used published proteomics and flux data from chemostats for model evaluation, and
20 simulated glucose-limited conditions by minimizing the glucose concentration at a fixed
21 specific growth rate with an upper bound on the expression of the glucose transporter. The
22 model predicted the glucose uptake rates well (Fig 1c) and indicated -as expected- increased
23 saturation of the glucose transporter with growth rate (Fig 1d). Additionally, pcLactis
24 predicted overflow metabolism, i.e., a metabolic switch from mixed acid to lactic acid
25 fermentation, corresponding to simultaneous changes at the proteome level (Fig S1a), but at
26 a much higher growth rate than experimentally observed (Fig 1c). However, experimental
27 evidence showed that the metabolic switch in *L. lactis* does not relate to considerable
28 proteome changes[3] and therefore the switch predicted by pcLactis might probably not reflect
29 the true reason for overflow metabolism; The metabolic switch rather involves enzyme
30 kinetics that are beyond the current stoichiometric model (see[24] for a possible explanation).
31 More importantly, the model predicted that at a dilution rate (D) higher than 0.5 h^{-1}, the
32 fraction of inactive enzyme becomes zero (Fig 1e). This means that at that point all proteins
33 are maximally active and any flux change can only be brought about by changes in protein
34 levels, not enzyme saturation. The proteomics data showed genome-wide protein reallocation
35 when growth rate increased beyond that point[3], validating the model prediction.
36
37 To identify the "active" constraints, i.e., constraints that limit the growth rate in pcLactis, we
38 developed a sensitivity analysis for proteome-constrained models. Glucose transport
39 expression was an active constraint at low growth rates and its sensitivity dropped at the
40 moment the inactive protein reached zero (Fig 1f); At that point, the total proteome also
41 became limiting. This reflects the increased demand in proteome resource at high growth
42 rates, both for metabolic fluxes and protein translation machinery (Fig S1a). Thus, around D =
43 0.5 h^{-1}, the model switched from glucose-limited to combined glucose and proteome limited.
44
45 In the model, the transition to proteome limited growth was reflected in amino acid
46 metabolism, not overflow metabolism. However, including amino acid uptake in pcLactis was
47 challenging as the amino acid consumption could not be constrained by the model due to

1   insufficient data of expression and kinetics for amino acid transport systems. This would thus
2   lead to an overestimation of uptake and growth rate when setting free exchange rates of all
3   20 amino acids to mimic the medium of *L. lactis*, where amino acids are mostly in excess.
4   However, published amino acid data[3] showed that apart from aspartate and glutamate all the
5   detected amino acids were taken up linearly with growth rate (Fig 2a). We therefore imposed
6   growth rate-dependent upper bounds on the uptake rates of all amino acids based on these
7   measurements. To distinguish anabolism and catabolism, we compared the uptake of amino
8   acids with their tRNA charging flux, which represents the flux towards protein synthesis. To
9   analyse the results, we performed a so-called scaled reduced cost analysis, which is a
10 sensitivity analysis of the uptake bounds on the growth rate (Fig 2b).

11

12 The predicted uptake fluxes of most amino acids follow the upper bound set by the
13 experimental data. Many of those amino acids were overconsumed and thus catabolized, in
14 agreement with model predictions (Fig 2a). Based on the scaled reduced cost analysis, their
15 catabolism contributed to growth rate (the mechanistic basis of many of those were
16 previously analysed for *Lactobacillus plantarum*[25]). Those amino acids with little impact on
17 growth rate, based on the scaled reduced cost analysis, are taken up by *L. lactis* according to
18 protein synthesis demand. Thus, pcLactis can explain overconsumption of specific amino acids
19 according to growth rate optimisation. This is interesting, as many of the catabolic products
20 contribute to flavour formation in food fermentations. Leucine, tryptophan and to a lesser
21 extent valine were exceptions (Fig 2a). In *L. plantarum* leucine and valine catabolism
22 contributes to the redox balance, which requires a NADP-dependent glutamate
23 dehydrogenase[25]; *L. lactis*, however, lacks this enzyme[26]. The reason for overconsumption of
24 these amino acids thus remains to be unravelled.

25

26 When the total proteome becomes an active constraint at a growth rate around 0.5 h^{-1}, we
27 observe a drop in several amino acid overconsumptions in pcLactis. This is also reflected in a
28 drop in reduced cost of the respective amino acids (Fig 2), indicating that the metabolic benefit
29 was not high enough for the now constraining protein investment in the catabolic pathway.
30 Experimentally, not all amino acids dropped at this point, although data is more variable at
31 the highest growth rate. However, the most pronounced change in flux was observed for
32 arginine, the amino acid that also had the highest (drop in) reduced cost. Arginine is also the
33 only amino acid whose catabolism directly yields ATP. The predicted changes in the fluxes of
34 catabolic products ornithine and ammonium (Fig S1b), and the concomitant changes in
35 protein levels of the pathway (Fig S1a) together with experimental observations[3,19], confirm
36 that pcLactis correctly captured the switch in arginine catabolism.

37

38 We noted that the arginine switch preceded the onset of overflow metabolism (lactate) in
39 pcLactis (Fig S1c). We constructed a small model to analyse this switching behaviour,
40 expecting that protein efficiency, i.e. ATP produced per protein mass per time, was key[13]. We
41 defined three independent ATP-producing pathways, glycolysis pathway with mixed acid
42 fermentation or with lactate formation, and arginine catabolism (Fig 3a), and estimated ATP
43 yield, protein cost and protein efficiency (Fig 3b) for each pathway using pcLactis. With these
44 parameters, we formulated a linear program to maximize ATP production flux subject to total
45 proteome constraints with flux bounds (Fig 3c). We varied glucose uptake fluxes and found
46 three distinct phases: when the total proteome is not constrained both mixed acid
47 fermentation and arginine catabolism are used (phase A, Fig 3d), as mixed acid fermentation

1   has the highest ATP yield and arginine provides extra ATP at no protein burden. Once the total
2   proteome is constrained (phase B, Fig 3d), the flux through arginine catabolism goes down
3   due to its lowest protein efficiency. When arginine catabolism is completely inactive, mixed
4   acid fermentation is traded in for lactate formation (phase C, Fig 3d), as its protein efficiency
5   is lower than lactic acid fermentation. Furthermore, the small model reproduced the
6   sensitivity results in terms of the constraints on glucose and arginine uptake (Fig 3d). Thus,
7   the small model captures the behaviour of the full model, reinforcing earlier theoretical
8   results that the number and nature of the active constraints determine behaviour, irrespective
9   of the size of the network[24].

10
11 Since pcLactis uses optimisation, we investigated if the predicted high sensitivities for glucose
12 and arginine metabolism would provide targets for fitness improvements. For the simulations
13 we used previously experimentally determined constraints on the uptake of amino acids[3],
14 which could be suboptimal under glucose-limited chemostat conditions. We therefore
15 compared wild type *L. lactis* MG1363 with a mutant strain (designated 445C1) that evolved
16 from MG1363 under glucose-limited chemostat conditions at D = 0.5 h^{-1}, which harbours a
17 point mutation in the global carbon catabolite repression regulator (CcpA)[27]. This CcpA mutant
18 shows a twofold increase of mixed acid fermentation at the endpoint of the laboratory
19 evolution experiment, while fermentation towards lactate is decreased[27]. This change in
20 metabolism is consistent with the prediction that the total proteome constraint is not yet
21 active at 0.5 h^{-1}, as that would provide a driving force towards lactate formation (Fig 3).

22
23 To further validate predictions, we assessed protein allocation and amino acid metabolism of
24 wild type and CcpA mutant, not studied before. We therefore re-cultivated both strains in
25 glucose-limited chemostats at D = 0.5 h^{-1} and compared them at the proteome and metabolic
26 level (Fig 4a). Principal component analysis of the proteomics data confirmed reproducibility
27 (Fig S2). Apparent catabolic and total carbon balances were between 89 and 100%
28 (Supplementary Data 3). We also found increased mixed acid and decreased lactic acid
29 fermentation for the CcpA mutant compared to wild type (Fig S3), in agreement with the
30 published data[27].

31
32 The proteomics data showed that arginine catabolism, including its uptake system are
33 significantly upregulated in the CcpA mutant compared to the wild type (Fig 4b; Fig S4).
34 Consequently, we found an increased arginine uptake flux in the CcpA mutant (Fig 4c), to the
35 extent that no residual arginine was detected anymore in its supernatant (Fig 4d). Other amino
36 acids revealed no clear changes (Fig 4c, Fig S5), even though some had nonzero reduced costs
37 as well, likely because metabolism of these amino acids is not under control of CcpA[28]. Taken
38 together arginine could be the most effective amino acid on optimizing fitness under the
39 chosen conditions as predicted by our model.

40
41 We further found a significantly increased protein fraction of glucose transporters in the CcpA
42 mutant ($p < 0.001$) (Fig 4e), confirming that glucose uptake capacity was growth-limiting in
43 the wild type. Even though the total proteome is not limiting at D = 0.5 h^{-1}, we did find changes
44 in cytosolic protein fractions, notably the glycolysis fraction (Fig 4e), while other proteins, not
45 used by pcLactis under glucose limitation, were downregulated, e.g., peptide digestion and
46 NADH oxidases (Fig 4b, Fig S4). These may be part of the global catabolite repression effect of
47 the CcpA mutation without large fitness impact. Alternatively, upregulation of glycolysis may

relieve inhibition on glucose transport, such as the negative impact of fructose 1,6-bisphosphate on the PTS system, via HPr[29].

We did not find a considerable change in the total protein membrane fraction (Table S1), suggesting that the membrane protein occupancy is independent of the tested conditions and, given the need to transport many nutrients, possibly maximally occupied. If fully occupied, an increase of one protein would go at the cost of another protein. In the CcpA mutant we found an overrepresentation of significantly changed membrane proteins (p = 0.030 compared to random distribution of significantly changed proteins over membrane and cytosolic protein fraction, Table S1), amongst which downregulation of unused transport systems such as for peptides (Opp operon in Fig 4b). The idea that the membrane is fully occupied with proteins would also explain why amino acid uptake is not higher in wild type. It is therefore anticipated to impose a constraint on total membrane proteins in future simulations when transporter kinetics are available.

In conclusion, we show that integration of flux and proteomics data with a proteome-constrained genome-scale model allows for advanced sensitivity analysis of growth in complex nutrient environments. These sensitivities are predictive for evolutionary change, providing deeper understanding of the driving forces that shape regulatory strategies. We find changes in sensitivity that reflect which constraints become active under different growth rate regimes. Rather than the shift between mixed acid and lactic acid fermentation, we show that arginine metabolism, the third ATP yielding pathway in *L. lactis* and many other bacteria, is subject to proteome-constraint driven protein reallocation, mediated by CcpA. And after all, also *L. lactis* appears to abide to the microbial growth laws[30] of cellular resource allocation.

Methods
Proteome-constrained model construction. The detailed construction procedure is described in the Supplementary Note. Firstly, we updated the existing genome-scale metabolic model of *L. lactis* MG1363[21,22] in terms of transport reactions and gene-protein-reaction (GPR) associations by using MetaDraft (http://doi.org/10.5281/zenodo.2398336), a tool that reconstructs genome-scale metabolic networks based on previous manually curated ones by homology between genes, and subsequently manual curation. For non-spontaneous reactions with missing GPRs, we assigned a "dummy" protein as their catalysts to eliminate potential bias toward using them in simulations. Then we split reactions with isozymes into multiple reactions that each is catalysed by one isozyme, and reversible reactions into forward and reverse direction. In addition to updating and reformulating metabolic reactions, we formulated reactions for transcription, stable RNA cleavage, mRNA degradation, tRNA modification, rRNA modification, tRNA charging, ribosomal assembly, translation, protein maturation, protein assembly, enzyme formation, and protein degradation. Additionally, we formulated dilution reactions for RNA and enzymes to represent their dilution to daughter cells during cell division. Lastly, we modified the biomass equation of the metabolic model, i.e., removed protein and RNA from the equation as they were represented by dilution reactions, and added an unmodelled protein to account for all the other proteins that are not synthesized by the model. The genome-scale metabolic model was updated using CBMPy (https://doi.org/10.5281/zenodo.3485023), while pcLactis was constructed using the COBRA toolbox[31].

1   **Constraints and kinetics parameters.** In addition to classical constraints of GEMs, e.g., mass
2   balance and bounds on reaction rates, two protein constraints are imposed including a fixed
3   bound on the total modelled proteome and an upper bound on the abundance of glucose
4   transporter (Supplementary Note). The fraction of modelled proteome was estimated
5   according to the PaxDb database[23], where abundance of each protein is collected. The data is
6   however available only for *L. lactis* IL1403, and thus we performed BLASTp for mapping
7   protein IDs between *L. lactis* IL1403 and MG1363. As a result, we obtained a list of proteins in
8   *L. lactis* MG1363 with available abundance data (Supplementary Data 2). It should be noted
9   that we filtered out the proteins of blocked reactions that would never carry fluxes in the
10 model.
11
12 Besides, pcLactis accounts for coupling constraints that relate enzymes and machineries to
13 their catalytic functions. In pcLactis such constraints are imposed for coupling enzymes to
14 metabolic reactions, RNA polymerase to transcription reactions, ribosomes to translation
15 reactions, and so on. All the coupling constraints are detailed in the Supplementary Note. In
16 order to determine coefficients in the coupling constraints, we automatically retrieved
17 turnover rates of metabolic enzymes from the BRENDA database[32] using the GECKO toolbox[12]
18 but also manually adjusted some according to literatures. Besides, we estimated catalytic
19 rates of gene expression machineries, including ribosome, RNA polymerase, mRNA and tRNA,
20 in the same way as done for ME-Model of *E. coli*[9] based on reported data[20,33] for *L. lactis*.
21 Detailed description can be found in the Supplementary Note.
22
23 **Simulations with pcLactis for anaerobic glucose-limited conditions.** Since growth rate is
24 integrated into coupling constraints in linear programming, it should be used as input for
25 simulations. Therefore, we used a binary search workflow to obtain the minimal extracellular
26 glucose concentration that leads to a feasible solution for any given growth rate to simulate
27 glucose-limited conditions. This approach is based on the Michaelis-Menten equation with a
28 fixed upper limit on the concentration of the glucose transporter:

29
$$q_S = k_{cat}[E]\sigma = k_{cat}[E]\frac{S}{K_M + S}, [E] \leq upper\ bound$$

30 in which q_S is the glucose uptake rate, k_{cat} is the turnover rate of the glucose transporter
31 adopted from *E. coli*[34], $[E]$ is the concentration of the glucose transporter, σ is the saturation
32 of the glucose transporter, S is the extracellular glucose concentration and K_M is the
33 Michaelis constant obtained from the study[27]. The upper bound on the concentration of the
34 glucose transporter was estimated using pcLactis, i.e., the minimal concentration that gives a
35 feasible solution for the maximal growth rate. According to the Michaelis-Menten equation,
36 searching for the minimal extracellular glucose concentration is equal to searching for the
37 lowest saturation σ, which is equivalent to minimizing the glucose uptake rate when the upper
38 bound of the concentration of the glucose transporter is hit.
39
40 The binary search solved successive individual linear programs, which maximizes the
41 production of the dummy protein subject to stoichiometric and coupling constraints. Lower
42 and upper bounds of some reactions were also constrained. Notably, amino acid exchange
43 fluxes were constrained by growth rate-dependent upper bounds based on experimental
44 data[3]. Besides, biomass dilution reaction, which represents the dilution of other biomass
45 components than modelled protein and RNA, was fixed according to the growth rate. Due to
46 the anaerobic condition we blocked two reactions, i.e., oxygen exchange reaction and

7

1 pyruvate oxidase reaction. In addition, we blocked one alcohol dehydrogenase reaction
2 catalysed by the isozyme llmg_0955, and two glucose transport reactions due to low protein
3 levels[3]. Simulations were solved using Soplex 4.0.0 (https://soplex.zib.de/).
4
5 **Small model and simulations.** The small model was extracted from pcLactis, which contains
6 three pathways including glycolysis pathway with mixed acid fermentation, glycolysis pathway
7 with lactic acid fermentation and arginine catabolism.
8
9 We estimated ATP yield, protein cost and protein efficiency for each pathway. Firstly, we
10 identified the flux distribution of each pathway by solving a linear program with the metabolic
11 part of pcLactis. For each simulation, the upper bound on ATP maintenance reaction was set
12 free in order to account for ATP consumption. For mixed acid fermentation, the linear program
13 is to maximize ATP maintenance reaction subject to a fixed glucose uptake rate of 1
14 mmol/gCDW/h. For lactate acid fermentation, the linear program is to maximize lactate
15 production subject to a fixed glucose uptake rate of 1 mmol/gCDW/h and ATP maintenance
16 reaction rate of 2 mmol/gCDW/h. For arginine catabolism, the linear program is to maximize
17 ATP maintenance reaction subject to a fixed arginine uptake rate of 1 mmol/gCDW/h.
18 Accordingly, we calculated ATP yield for each pathway, i.e., the flux of ATP maintenance
19 reaction over uptake rate of substrate. Secondly, we estimated the protein cost for each
20 pathway based on the flux distribution, which is the protein cost of each reaction in the
21 pathway times the corresponding flux value. The protein cost of a reaction is molecular weight
22 of the corresponding enzyme over its turnover rate[13], and therefore can be extracted from
23 pcLactis. Lastly, the protein efficiency of each pathway is ATP yield over protein cost.
24
25 With the parameters, we generated a linear program of fluxes through the three pathways,
26 which is to maximize ATP production flux subject to constraints on uptake fluxes of substrates,
27 i.e., glucose and arginine, and total proteome. We performed the simulations for a wide range
28 of glucose uptake fluxes.
29
30 **Scaled reduced cost analysis.** We performed the scaled reduced cost analysis[25] for uptake
31 rate of each amino acid on growth rate with pcLactis. The scaled reduced cost R_i of the growth
32 rate μ_i with respect to the uptake rate of an amino acid q_i is calculated as: $R_i = (\Delta\mu/\Delta q)(q_i/\mu_i)$. We imposed a small increase in the uptake rate of each amino acid $\Delta q = 0.01$ to investigate the change in growth rate $\Delta\mu$.
33
34
35
36 **Sensitivity analysis.** We performed sensitivity analysis for two constraints with pcLactis, i.e.,
37 the glucose transporter and modelled proteome, on growth rate. The sensitivity score S_i of
38 the growth rate μ_i with respect to a given constraint c_i is calculated as: $S_i = (\Delta\mu/\Delta c)(c_i/\mu_i)$.
39 With pcLactis, we imposed a small increase $\Delta c = 0.01$ in the glucose transporter and
40 modelled proteome to investigate the change in growth rate $\Delta\mu$ at different conditions. We
41 also performed sensitivity analysis with the small model for glucose uptake, proteome
42 allocated to the small model and arginine uptake using the small increase $\Delta c = 0.01$ to
43 investigate the change in ATP production rate q_{ATP}, i.e., the sensitivity score S_i is calculated
44 as: $S_i = (\Delta q_{ATP}/\Delta c)(c_i/q_{ATP})$.
45
46 **Strains and media.** *Lactococcus lactis* ssp. *cremoris* MG1363 is a plasmid cured derivative of
47 strain NCDO712[35,36]. Strain 445C1 is a derivative of MG1363 isolated after prolonged

1 cultivation in a chemostat[27]. Cultivation of strains were performed in chemically defined
2 medium for prolonged cultivation (CDMpc)[27] , supplemented with 25 mM glucose as limiting
3 carbon source at 30°C.
4
5 **Chemostat cultivation.** Proteome, metabolite and amino acid samples were obtained from
6 four steady state chemostats. Chemostat cultivation took place in 300 mL bioreactors with
7 270 mL working volume, under continuous stirring (using magnetic stirrers), while standing in
8 30°C water baths. The headspace was continuously flushed with 5% CO_2 and 95% N_2. pH was
9 controlled at 6.5 using 2.5 M NaOH. The pH probe was calibrated before and after the pre-
10 culture in the reactor. CDMpc with 25 mM glucose was added at a rate of 2.25 mL/min.
11 Superfluous liquid was continuously removed from the top of the reactor to maintain a
12 volume of 270 mL. This results in a dilution rate of 0.5 h^{-1}. The flow rate of each medium pump
13 was calibrated right before inoculating the reactor and checked again at the end of the
14 experiment. The exact volume of liquid in each reactor was determined at the end of the
15 experiment by weighing the reactor liquid.
16
17 To start up a chemostat culture, 5 mL CDMpc with 25 mM glucose was inoculated with glycerol
18 stocks of the respective strains, taken from a -80°C. This was directly added to the reactor
19 containing 265 mL fresh 25 mM glucose CDMpc. The reactor was operated in batch mode (no
20 medium addition, pH regulated, effluent pump on, 30 °C, continuous stirring, headspace
21 sparged) for 24 hours, allowing the cells to reach the stationary phase. This was verified by
22 observing that the pH remained constant without addition of 2 M NaOH. After 24 hours the
23 medium pump was switched on. The chemostat was operated for 8 volume changes before
24 samples were taken. Samples were taken from the effluent of the reactor. Retention time in
25 the effluent tube was <2 minutes. Sample tubes were kept on ice while sample was being
26 collected. For each strain four replicate chemostats were cultivated.
27
28 **Sampling procedures and measurements.** For extracellular metabolite concentration
29 measurements (for both reactor broth and sterile medium), 2 mL samples were centrifuged
30 at 27237 G for 3 minutes at 4 °C, the supernatant was filtered through a 0.22 μm polyether
31 sulfone filter (VWR international) and stored at -20 °C until further analysis. Extracellular
32 concentrations of lactate, acetate, formate, ethanol and glucose were determined by high-
33 performance liquid chromatography (HPLC) as described previously[37].
34
35 Extracellular concentrations of amino acids were determined by HPLC on a Shimadzu system
36 with: LC-20AD pumps, DGU-14A degasser, SIL-10ADvp autosampler, CTO-10ASvp oven, SCL-
37 10Avp system controller, and RF-10AXL fluorescence detector. Separation occurred on an
38 Agilent Zebra Eclipse plus solvent saver 3.0x150x3.5 column over a period of 38 minutes per
39 sample, with an isocratic flow of two eluents both at a flow rate of 0.64 mL/min. Eluent 1 had
40 composition: 0.142 % w/v $NaHPO_4$, 0.381% w/v $Na_2B_4O_7 \cdot 10H_2O$, 0.0325% w/v sodium azide in
41 deionized water (DI water); and eluent 2 had composition: 45% v/v methanol, 45% v/v
42 acetonitrile in DI water. Samples were prepared by mixing 25 μL sample with 875 μL DI water,
43 25 μL Borate buffer (0.6% w/v boric acid, 0.4% w/v NaOH, pH 10.2), and 25 μL 1mM Norvaline
44 as internal standard. For amino acid derivation 3 μL phthaldialdehyde (Sigma-Aldrich), i.e.
45 OPA, was automatically added 3 minutes before sample injection (5 μL) into the column.
46 Concentrations were determined by comparison of sample peak areas to those of a calibration
47 curve identically run with representative amino acid concentrations.

Proteome samples were collected in low protein binding tubes, centrifuged at 27237 G for 3 minutes at 4°C. The supernatant was discarded, and the pellet was frozen in liquid N_2 prior to storage at -20°C until further analysis.

For dry weight measurements, 10 mL broth was collected and filtered over a pre-dried (3 days, 60 °C) pre-weighed 0.2 µm cellulose nitrate filter (Whatman GmbH). The filter was then washed once with 10 mL demineralized water and dried (3 days, 60°C), before weighing again.

Fluxes (q_i in mmol/gCDW/h) were calculated as: $q_i = D \cdot (C_{i,supernatant} - C_{i,medium})/ X_{biomass}$, where D is the dilution rate (h^{-1}), C the concentration of compound i (mmol/L) and $X_{biomass}$ the biomass concentration (g/L).

Proteome measurements. Proteins were isolated using the FASP method as described previously[38]. In short, cell pellets were dissolved in 100 mM TRIS pH 8 to a concentration of 7.5E8 cells/100 µl and lysed using a needle sonicator (MPE). Proteins obtained from 4.5E8 lysed cells were reduced with 15 mM dithiothreitol for 30 minutes at 45 °C and subsequently alkylated in 20 mM acrylamide for 10 minutes at room temperature under denaturing conditions (100 mM TRIS pH8 + 8 M Urea). The alkylated sample was transferred to an ethanol-washed Pall 3K omega filter (Sigma-Aldrich, The Netherlands) and centrifuged for 36 minutes at 12000 rpm. The filters were washed with 130 µl 50 mM ammonium bicarbonate and centrifuged again before overnight digestion with 100 µl 5 ng/µl trypsin (Roche) at room temperature. The digested peptides were eluted by centrifugation for 30 min, subsequent addition of 100 µl 1 ml/l HCOOH in water and again centrifugation for 30 min. pH was adjusted to pH 3 using trifluoroacetic acid.

MS/MS analysis was done as described previously[39]. Raw datafiles were analyzed using MaxQuant (version 1.6.1.0) and searched against the *L. lactis* MG1363 database (UniProt) and frequently observed contaminants. In addition to the standard settings, Trypsin/P with a maximum of two missed cleavages was set as the digestion mode, acrylamide modifications on the cysteines was set as a fixed modification, and methionine oxidation, protein N-terminal acetylation and asparagine or glutamine deamidation were set as variable modifications. A false discovery rate of 1% at protein level was allowed and the minimum required protein length was set at 7. At least two peptides were required for protein identification of which at least one peptide was required to be unique in the database. Identified proteins were quantified.

Proteomics data analysis. Statistical analysis on the MaxQuant output was performed with Perseus version 1.6.2.1. Proteins were accepted when they were represented in at least three of the four biological replicates in at least one strain. For statistical analysis log10 transformed LFQ values were used and zero values were replaced by taking random values from a normal distribution with mean (measured values per biological sample -1.8) and variation (0.3 * standard deviation of the measured values per biological replicate) to make calculations possible. We then performed a 2-sided two sample t-tests using the log10 normalized LFQ intensity columns of CcpA mutant and wild type with a FDR threshold of 0.05 and S_0 equal to 1[40]. Fold changes of CcpA mutant over wild type were calculated by dividing LFQ intensity columns of CcpA mutant by wild type. A principal component analysis of the LFQ data was

1   used to assess the reproducibility of the data. Further analysis steps were done with Python.
2   For fractions of protein groups, we used sums of intensity-based absolute quantitation (iBAQ)
3   protein fractions, which were obtained by normalizing iBAQ values by the total sum of all
4   values per biological replicate. Two-sided two sample t-tests were performed on biological
5   groups of proteins between the wild type and CcpA mutant strain. Furthermore, a two-sided
6   Fisher exact test was performed on the number of significantly changed proteins and
7   unchanged proteins in the membrane and rest of the cell. For this, the protein fractions were
8   first averaged over the biological replicates.
9

Data availability

11   The mass spectrometry proteomics data have been deposited to the ProteomeXchange
12   Consortium via the PRIDE[41] partner repository with the dataset identifier PXD021956.
13

Code availability

15   The model and codes are available online at https://github.com/SysBioChalmers/pcLactis.
16

Acknowledgements

24

Author contributions

26   B.T., H.B. and J.N. conceived the study. Y.C. and E.v.P.-K. performed the modelling, simulations
27   and data-analysis. B.v.O. and S.D. performed experiments. D.M. and S.B. contributed to the
28   data-analysis. Y.C., E.v.P.-K and B.T. wrote the manuscript. All authors contributed to
29   manuscript editing.
30

Competing interests

32   The project is organised by and executed under the auspices of TiFN, a public – private
33   partnership on precompetitive research in food and nutrition. The authors have declared that
34   no competing interests exist in the writing of this publication.
35   Funding for this research was obtained from Friesland Campina, CSK Food Enrichment, the
36   Netherlands Organisation for Scientific Research and the Top-sector Agri&Food.
37
38
39

Reference

1. Goel, A., Wortel, M. T., Molenaar, D. & Teusink, B. Metabolic shifts: a fitness perspective for microbial cell factories. *Biotechnol. Lett.* **34**, 2147–2160 (2012).

2. Basan, M. Resource allocation and metabolism: the search for governing principles. *Curr. Opin. Microbiol.* **45**, 77–83 (2018).

3. Goel, A. *et al.* Protein costs do not explain evolution of metabolic strategies and regulation of ribosomal content: does protein investment explain an anaerobic bacterial Crabtree effect? *Mol. Microbiol.* **97**, 77–92 (2015).

4. Chubukov, V., Gerosa, L., Kochanowski, K. & Sauer, U. Coordination of microbial metabolism. *Nat. Rev. Microbiol.* **12**, 327–340 (2014).

5. Beg, Q. K. *et al.* Intracellular crowding defines the mode and sequence of substrate uptake by Escherichia coli and constrains its metabolic activity. *Proc. Natl. Acad. Sci.* **104**, 12663–12668 (2007).

6. Molenaar, D., van Berlo, R., de Ridder, D. & Teusink, B. Shifts in growth strategies reflect tradeoffs in cellular economics. *Mol. Syst. Biol.* **5**, 323 (2009).

7. de Groot, D. H. *et al.* The common message of constraint-based optimization approaches: overflow metabolism is caused by two growth-limiting constraints. *Cellular and Molecular Life Sciences* **77**, 441–453 (2020).

8. Zhuang, K., Vemuri, G. N. & Mahadevan, R. Economics of membrane occupancy and respiro-fermentation. *Mol. Syst. Biol.* **7**, 500 (2011).

9. O'Brien, E. J., Lerman, J. A., Chang, R. L., Hyduke, D. R. & Palsson, B. Genome-scale models of metabolism and gene expression extend and refine growth phenotype prediction. *Mol. Syst. Biol.* **9**, 693 (2013).

10. Basan, M. *et al.* Overflow metabolism in Escherichia coli results from efficient proteome allocation. *Nature* **528**, 99–104 (2015).

11. Nilsson, A. & Nielsen, J. Metabolic Trade-offs in Yeast are Caused by F1F0-ATP synthase. *Sci. Rep.* **6**, 22264 (2016).

12. Sánchez, B. J. *et al.* Improving the phenotype predictions of a yeast genome-scale metabolic model by incorporating enzymatic constraints. *Mol. Syst. Biol.* **13**, 935 (2017).

13. Chen, Y. & Nielsen, J. Energy metabolism controls phenotypes by protein efficiency and allocation. *Proc. Natl. Acad. Sci. U. S. A.* **116**, 17592–17597 (2019).

14. Papadimitriou, K. *et al.* Stress Physiology of Lactic Acid Bacteria. *Microbiol. Mol. Biol. Rev.* **80**, 837–90 (2016).

15. Kok, J. *et al.* The Evolution of gene regulation research in Lactococcus lactis. *FEMS Microbiol. Rev.* **41**, S220–S243 (2017).

16. Teusink, B. & Molenaar, D. Systems biology of lactic acid bacteria: For food and thought. *Curr. Opin. Syst. Biol.* **6**, 7–13 (2017).

17. Jensen, P. R. & Hammer, K. Minimal Requirements for Exponential Growth of Lactococcus lactis. *Appl. Environ. Microbiol.* **59**, (1993).

18. Fernández, M. & Zúñiga, M. Amino Acid Catabolic Pathways of Lactic Acid Bacteria. *Crit. Rev. Microbiol.* **32**, 155–183 (2006).

19. Crow, V. L. & Thomas, T. D. Arginine metabolism in lactic streptococci. *J. Bacteriol.* **150**, 1024–1032 (1982).

20. Novák, L. & Loubiere, P. The metabolic network of Lactococcus lactis: Distribution of 14C- labeled substrates between catabolic and anabolic pathways. *J. Bacteriol.* **182**, 1136–1143 (2000).

1 21. Flahaut, N. A. L. *et al.* Genome-scale metabolic model for Lactococcus lactis MG1363
2   and its application to the analysis of flavor formation. *Appl. Microbiol. Biotechnol.* **97**,
3   8729–8739 (2013).
4 22. Verouden, M. P. H. *et al.* Multi-way analysis of flux distributions across multiple
5   conditions. *J. Chemom.* **23**, 406–420 (2009).
6 23. Wang, M., Herrmann, C. J., Simonovic, M., Szklarczyk, D. & von Mering, C. Version 4.0
7   of PaxDb: Protein abundance data, integrated across model organisms, tissues, and
8   cell-lines. *Proteomics* **15**, 3163–3168 (2015).
9 24. de Groot, D. H., van Boxtel, C., Planqué, R., Bruggeman, F. J. & Teusink, B. The number
10   of active metabolic pathways is bounded by the number of cellular constraints at
11   maximal metabolic rates. *PLOS Comput. Biol.* **15**, e1006858 (2019).
12 25. Teusink, B. *et al.* Analysis of growth of Lactobacillus plantarum WCFS1 on a complex
13   medium using a genome-scale metabolic model. *J. Biol. Chem.* **281**, 40041–8 (2006).
14 26. Wels, M., Siezen, R., Van Hijum, S., Kelly, W. J. & Bachmann, H. Comparative genome
15   analysis of Lactococcus lactis indicates niche adaptation and resolves
16   genotype/phenotype disparity. *Front. Microbiol.* **10**, 4 (2019).
17 27. Price, C. E. *et al.* Adaption to glucose limitation is modulated by the pleotropic
18   regulator CcpA, independent of selection pressure strength. *BMC Evol. Biol.* **19**, 15
19   (2019).
20 28. Zomer, A. L., Buist, G., Larsen, R., Kok, J. & Kuipers, O. P. Time-resolved determination
21   of the CcpA regulon of Lactococcus lactis subsp. cremons MG1363. in *Journal of*
22   *Bacteriology* **189**, 1366–1381 (American Society for Microbiology Journals, 2007).
23 29. Deutscher, J., Francke, C. & Postma, P. W. How Phosphotransferase System-Related
24   Protein Phosphorylation Regulates Carbohydrate Metabolism in Bacteria. *Microbiol.*
25   *Mol. Biol. Rev.* **70**, 939–1031 (2006).
26 30. Scott, M., Gunderson, C. W., Mateescu, E. M., Zhang, Z. & Hwa, T. Interdependence of
27   cell growth and gene expression: origins and consequences. *Science* **330**, 1099–102
28   (2010).
29 31. Heirendt, L. *et al.* Creation and analysis of biochemical constraint-based models using
30   the COBRA Toolbox v.3.0. *Nat. Protoc.* 1 (2019). doi:10.1038/s41596-018-0098-2
31 32. Jeske, L., Placzek, S., Schomburg, I., Chang, A. & Schomburg, D. BRENDA in 2019: a
32   European ELIXIR core data resource. *Nucleic Acids Res.* **47**, D542–D549 (2019).
33 33. Beresford, T. & Condon, S. Physiological and genetic regulation of rRNA synthesis in
34   Lactococcus. *J. Gen. Microbiol.* **139**, 2009–2017 (1993).
35 34. Szenk, M., Dill, K. A. & de Graff, A. M. R. Why Do Fast-Growing Bacteria Enter
36   Overflow Metabolism? Testing the Membrane Real Estate Hypothesis. *Cell Syst.* **5**, 95–
37   104 (2017).
38 35. Gasson, M. J. Plasmid complements of Streptococcus lactis NCDO 712 and other lactic
39   streptococci after protoplast-induced curing. *J. Bacteriol.* **154**, (1983).
40 36. Wegmann, U. *et al.* Complete genome sequence of the prototype lactic acid
41   bacterium Lactococcus lactis subsp. cremoris MG1363. *J. Bacteriol.* **189**, 3256–70
42   (2007).
43 37. Goel, A., Santos, F., Vos, W. M. de, Teusink, B. & Molenaar, D. Standardized assay
44   medium to measure Lactococcus lactis enzyme activities while mimicking intracellular
45   conditions. *Appl. Environ. Microbiol.* **78**, 134–43 (2012).
46 38. Wiśniewski, J. R., Zougman, A., Nagaraj, N. & Mann, M. Universal sample preparation
47   method for proteome analysis. *Nat. Methods* **6**, 359–362 (2009).

39. Sotoca, A. M. *et al.* Quantitative Proteomics and Transcriptomics Addressing the Estrogen Receptor Subtype-mediated Effects in T47D Breast Cancer Cells Exposed to the Phytoestrogen Genistein. *Mol. Cell. Proteomics* **10**, M110.002170 (2011).

40. Tusher, V. G., Tibshirani, R. & Chu, G. Significance analysis of microarrays applied to the ionizing radiation response. *Proc. Natl. Acad. Sci. U. S. A.* **98**, 5116–5121 (2001).

41. Vizcaíno, J. A. *et al.* 2016 update of the PRIDE database and its related tools. *Nucleic Acids Res.* **44**, D447–D456 (2016).
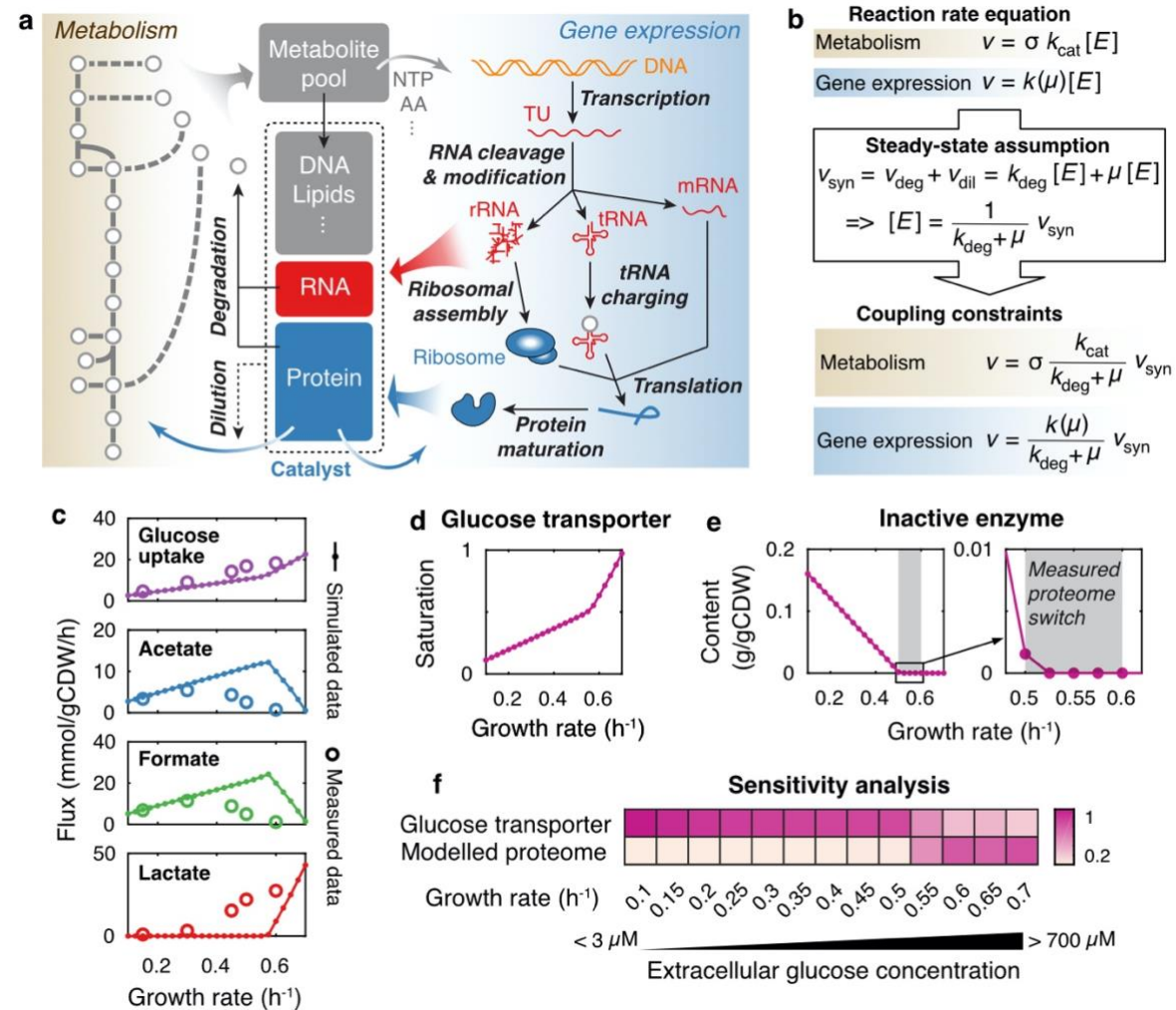
1   **Figure legend**

2
3   **Fig1. Overview of pcLactis and simulations of glucose-limited conditions. a,** The model
4   explicitly accounts for reactions of metabolism and gene expression processes. Metabolic
5   reactions produce metabolites and energy for not only biomass formation but also gene
6   expression processes. The reactions of gene expression, on the other hand, synthesize RNA
7   and proteins, which catalyse reactions of metabolism and gene expression processes as
8   machineries or enzymes. Besides, pcLactis accounts for degradation of mRNA and proteins as
9   well as dilution of biomass constituents during cell division. **b,** Coupling constraints in pcLactis.
10   The coupling constraint allows for relating the reaction rate to the synthesis rate of its catalyst
11   based on the reaction rate equation and steady-state assumption, where turnover rates k_{cat}
12   of metabolic enzymes, catalytic rates k of machineries and degradation constants k_{deg} of the
13   catalysts are needed. **c,** Simulated exchange fluxes compared with experimentally measured
14   data[3]. **d,** Simulated saturation of glucose transporter. **e,** Simulated inactive enzyme. The
15   inactive enzyme is the sum of the enzymes that are synthesized but do not carry fluxes. The
16   production of the inactive enzyme indicates that total proteome is not constrained. The grey
17   area represents where the proteome switch occurs in experiments[3], which is between 0.5 and
18   0.6 h^{-1}. **f,** Sensitivity analysis for glucose transporter and modelled proteome at different
19   growth rates. Colour represents the sensitivity score. A higher score indicates a greater impact
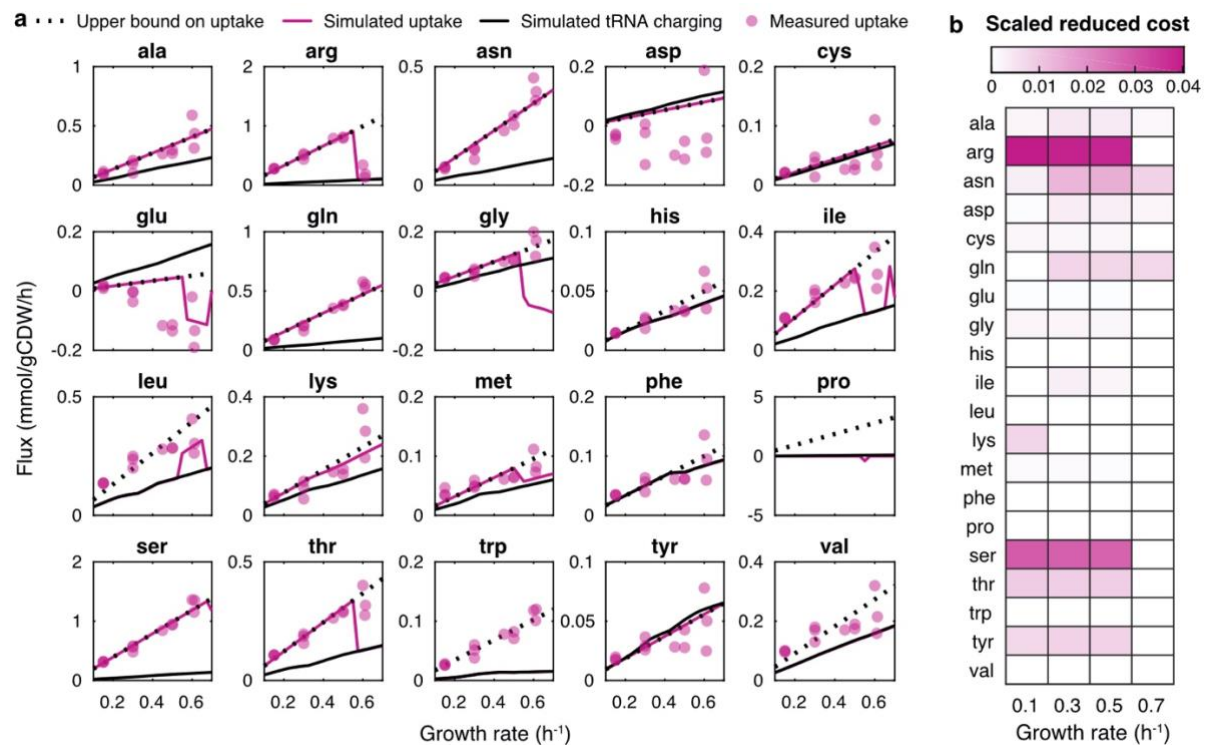20   of a given increase in the constraint on growth rate.
21

Fig2. Amino acid analysis with pcLactis shows importance of amino acid catabolism for growth as a function of active constraints. a, Simulated fluxes of amino acids compared with experimentally measured data. For each amino acid, simulated fluxes of uptake and tRNA charging are displayed together with the measured uptake flux. The upper bound on the uptake is also displayed, which is the linear trendline of the experimentally measured data if the amino acid is consumed rather than being secreted. The measured data are from the study[3]. **b,** Scaled reduced cost analysis for uptake rates of amino acids at different growth rates. Colour represents the scaled reduced cost value. A higher value indicates a greater impact of a given increase in the amino acid uptake on growth rate.
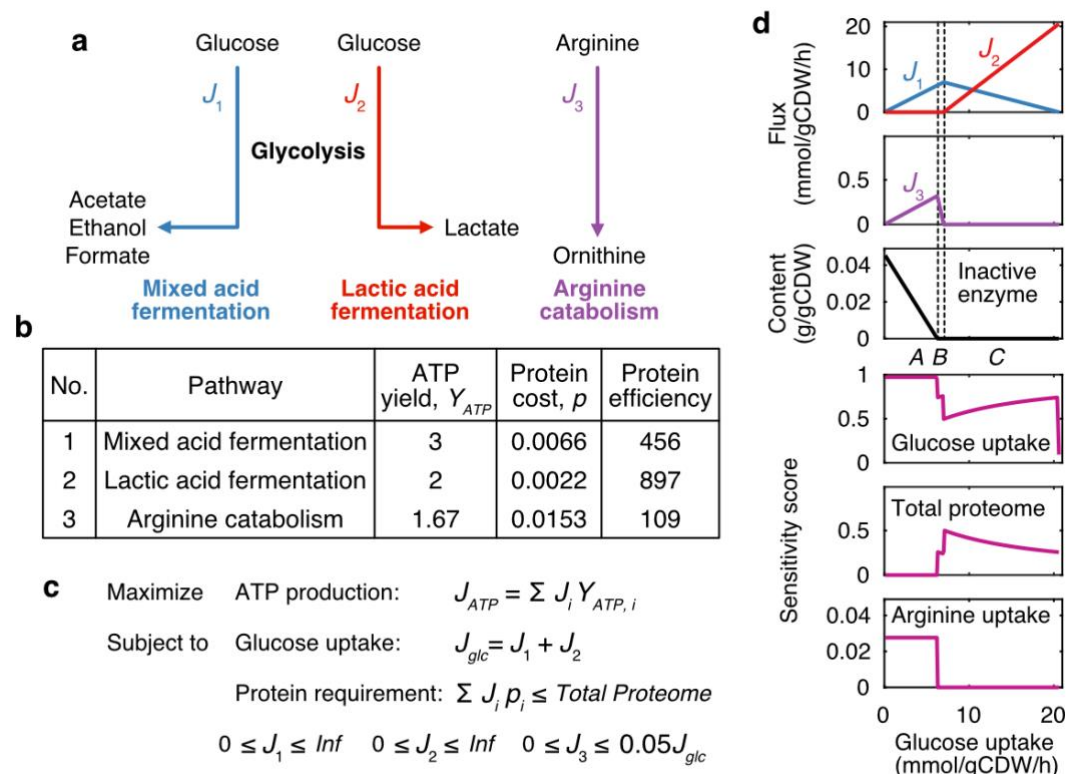
1
2 **Fig3. The switches between ATP yielding pathways in *L. lactis* can be explained from a**
3 **protein efficiency point of view. a,** A small model derived from pcLactis to investigate primary
4 ATP-producing pathways in *L. lactis*. The small model consists of three independent pathways,
5 including glycolysis pathway followed by mixed acid fermentation, glycolysis pathway
6 followed by lactic acid fermentation and arginine catabolism. **b,** Parameters of ATP-producing
7 pathways inferred from pcLactis. ATP yield is ATP generated per glucose (for pathway 1 and 2)
8 or arginine (for pathway 3) consumed. Protein cost is protein mass (unit: g/gCDW) required
9 per substrate flux (unit: mmol/gCDW/h) through the pathway. Protein efficiency is ATP
10 generated per protein mass per time with the unit of mmol of ATP per gram of protein per
11 hour. **c,** Linear programming to solve the small model. The objective function is to maximize
12 the total ATP production flux J_{ATP}, which is the sum of ATP production fluxes of three pathways
13 calculated by substrate uptake flux J_i times ATP yield $Y_{ATP,i}$. The model is subject to two
14 constraints. One is the total glucose uptake flux J_{glc}, which is the sum of the glucose fluxes
15 towards pathway 1 J_1 and 2 J_2. The other is the total proteome constraint, which means that
16 the sum of protein requirements of all pathways should be not greater than the proteome
17 allocation in the model. For each pathway, the protein requirement is calculated by the
18 protein cost p_i times substrate flux J_i. Besides, there are lower and upper bounds on the uptake
19 flux of each pathway. Specifically, J_1 and J_2 are unlimited while J_3 has a limited upper bound,
20 which is assumed to be linearly correlated with total glucose uptake flux J_{glc} based on
21 experimental observation. **d,** Small model simulations for a range of glucose uptake flux. The
22 top three plots show that with increasing glucose uptake flux the decline in arginine uptake
23 occurs firstly once the inactive enzyme disappears, and subsequently the switch from mixed
24 to lactic acid fermentation. The inactive enzyme is the difference between the total protein
25 requirements and the total proteome. The bottom three plots show sensitivities of glucose
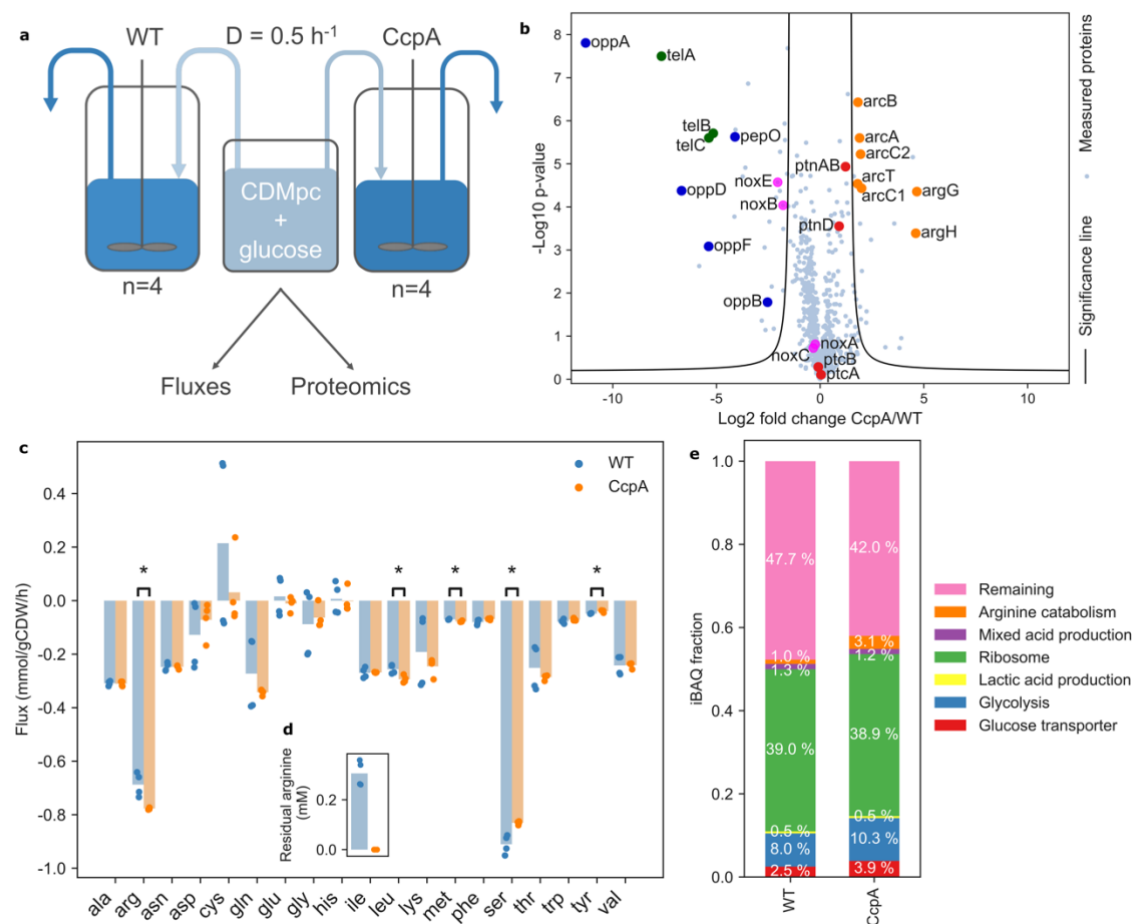26 uptake, total proteome and arginine uptake to the ATP production.
27

17

Fig4. Proteome of the CcpA mutant, which has a higher fitness than wild type *L. lactis*, is changed in the direction of optimality. a, Overview of experiments for comparing wild type *L. lactis* MG1363 and CcpA mutant 445C1 in glucose-limited chemostats at D = 0.5 h^{-1}. Samples were taken for dry weight measurements, external metabolite and amino acid analysis and proteome measurements. **b,** Protein fold changes of the CcpA mutant over wild type. Log2 fold changes were calculated from LFQ values *p* values were calculated based on 2-sided two sample t-tests with a FDR threshold of 0.05 and S$_0$ equal to 1[40]. Proteins outside the significance lines (FDR = 0.05, S$_0$ = 1) are significantly changed in expression. Example sets of proteins are highlighted and are labeled with their gene names. **c,** Amino acid fluxes (mmol/gCDW/h) and **d,** Residual concentration (mM) of arginine. The arginine uptake flux is increased to such extent that the residual arginine concentration became undetectable in the CcpA mutant. Data points represent the individual chemostats; bars are average values. **e,** Protein fractions. Protein fractions were obtained by normalizing iBAQ values by the total sum of all values. The obtained protein fractions were then averaged over the four biological replicates for visualization. The fractions glucose transport, glycolysis, arginine pathway and remaining fraction are significantly different between the two strains (*p* < 0.001, calculated with two-sided two sample t-tests).